JCTC Journal of Chemical Theory and Computation

Electron-Impact Ionization Cross Sections of Molecules Containing Heavy Elements ($Z > 10$)

Gregory E. Scott

Department of Chemistry, Davidson College, Davidson, North Carolina 28035-7120

Karl K. Irikura*

Computational Chemistry Group, National Institute of Standards and Technology, Gaithersburg, Maryland 20899-8380

Received March 25, 2005

Abstract: The binary-encounter-Bethe (BEB) theory has been successful for computing electron-impact ionization cross sections of many molecules. For molecules that contain heavy atoms (defined here as atoms with valence principal quantum number $n > 2$), there are two alternative BEB procedures in the literature. The first involves a kinetic-energy correction for molecular orbitals that are dominated by atomic orbitals with $n > 2$. The second alternative is to use effective core potentials (ECPs), which were developed for other purposes but yield valence pseudo-orbitals with reduced kinetic energies. In the present study, the results of these two approaches are compared with experimental cross sections for several molecules containing heavy elements. Although both procedures perform well, the ECP results agree somewhat better with experimental measurements. Cross sections are presented for C_2Cl_6, C_2HCl_5, C_2Cl_4, both isomers of $C_2H_2Cl_4$, CCl_4, $TiCl_4$, CBr_4, $CHBr_3$, CH_2Br_2, P_2, P_4, As_2, As_4, GaCl, CS_2, H_2S, CH_3I, $Al(CH_3)_3$, $Ga(CH_3)_3$, hexamethyldisiloxane, and $Zn(C_2H_5)_2$. Incorrect BEB calculations have been reported in the literature for several of these molecules. As an ancillary result, the dipole polarizability of $Zn(C_2H_5)_2$ is predicted to be 12.1 Å^3.

Introduction

Electron impact ionization cross sections are essential quantities for modeling plasma chemistry, which is important in a variety of practical processes. For example, low-temperature plasmas are important in semiconductor processing, in the destruction of volatile organic compounds, for modifying the mechanical properties of surfaces, and in wall-chemistry in nuclear fusion reactors. Absolute ionization cross sections are also necessary to obtain quantitative gas densities from mass-spectrometric measurements, as in flame sampling and Knudsen-cell thermochemistry.

Absolute ionization cross sections are difficult to measure precisely. Even for convenient, stable molecules, experimental groups often disagree on the values of the cross sections.[1] Furthermore, many of the interesting cross sections are for molecules that are especially difficult to measure, such as free radicals and molecular ions. Thus, reliable theoretical predictions are valuable.

The binary-encounter-Bethe (BEB) model[2,3] has been shown to produce reliable total cross sections for a wide variety of molecules.[4] For molecules containing heavy atoms, here meaning atoms with atomic number $Z > 10$, the ab initio computations required by the BEB model can be performed in two different ways: with all electrons explicit or by using core pseudopotentials, also known as effective core potentials (ECPs). Experimental cross sections are available for several such molecules,[5−7] warranting a comparison of the two computational approaches to BEB cross sections. Note that partial ionization cross sections, i.e., cracking patterns, cannot yet be predicted theoretically.

* Corresponding author phone: (301)975-2510; e-mail: karl.irikura@nist.gov.

10.1021/ct050077j CCC: $30.25
Published on Web 09/30/2005

Theoretical Procedures

In BEB theory, the total electron-impact ionization cross section is expressed as a sum of cross sections for each molecular orbital (MO)

$$\sigma_{\mathrm{MO}}(T;n) = \frac{S}{t + (u+1)/n}\left[\frac{\ln t}{2}\left(1 - \frac{1}{t^2}\right) + 1 - \frac{1}{t} - \frac{\ln t}{t+1}\right] \tag{1}$$

where T is the energy of the incident electron, $t = T/B$, $u = U/B$, $S = 4\pi a_0^2 N(R/B)^2$, a_0 is the Bohr radius, and R is the Rydberg energy. For each molecular orbital, B is the binding energy (i.e., the vertical ionization energy), U is the kinetic energy, and N is the number of electrons in the orbital (i.e., the occupation number). When $T < B$, the MO cannot be ionized, so $\sigma_{\mathrm{MO}} = 0$. The constant n is a kinetic-energy scaling factor whose role will be discussed below as it pertains to the two different methods of calculation. When B exceeds the second ionization energy (IE_2), the molecule is presumed to acquire a second charge through an Auger process. In that case, the contribution of σ_{MO} is doubled to correspond to experimental measurements of ion current, that is, the gross ionization cross section. For a molecule composed only of light atoms, eq 1 is used with $n = 1$ for all orbitals. When a molecule contains heavy atoms, there are two computational alternatives for applying the BEB model.

In the first method,[8] all electrons are included explicitly in the ab initio calculations. The scaling factor n in eq 1 is unity except for orbitals that are dominated by atomic orbitals with principal quantum number > 2, as judged by a Mulliken population greater than some threshold. When this is the case, n is set equal to the principal quantum number of the dominant atomic orbitals. We have typically used a threshold of 50%; choosing a different value generally changes the peak cross section by less than 10%.[1] However, changing the threshold affects the predicted cross sections systematically. As suggested by a referee, we consider the threshold as an adjustable parameter in this study.

In the second method,[9] the core electrons of the heavy atoms are replaced by effective potentials (ECPs). Since there are no core orbitals to which they must be orthogonal, the resulting valence pseudo-orbitals lack the radial nodes of normal orbitals, making their kinetic energies much lower than normal. [Nodes indicate oscillatory behavior, which corresponds to large gradients and curvatures in the orbital function. Eliminating radial nodes decreases the kinetic energy, especially in the core, because the principal radial dependence of the kinetic energy is proportional to $[\partial^2/\partial r^2 + (2/r)(\partial/\partial r)]$.[10]] Thus, eq 1 is used with $n = 1$ for all valence molecular pseudo-orbitals. No Mulliken populations or arbitrary thresholds are needed. However, since many core orbitals are missing in an ECP calculation, their contribution to the ionization cross section can only be obtained from a separate, all-electron calculation.

An intermediate situation sometimes arises in which certain orbitals do not lose any nodes upon introduction of an ECP. In the present study, this occurred for $Zn(C_2H_5)_2$. The 3*d* orbitals on Zn are considered to be valence orbitals and are treated explicitly even when an ECP is in use. However, 3*d* orbitals lack radial nodes, so their kinetic energy is nearly unaffected by using the ECP. Consequently, one should use $n = 3$ for the 3*d* orbitals even when an ECP is used. A similar situation would occur in the case of valence 4*f* orbitals.

Computational Methods[11]

All ab initio calculations in support of the BEB model were performed with the Gaussian 03 program suite using basis sets as implemented therein.[12] Basis sets listed in square brackets were used on atoms with atomic number $Z > 36$ (that is, beyond Kr). Molecular geometries were computed using the B3LYP hybrid density functional[13,14] with the 6-31G(d) [3-21G(d)] basis sets, with all electrons explicit. Vibrational frequencies were computed to verify that all structures are energy minima. These geometries were used for all subsequent calculations.

Orbital binding energies, B, kinetic energies, U [Gaussian 03 keyword iop(6/81=3)], and Mulliken populations were computed at the Hartree−Fock (HF) level using the 6-311G(d,p) [3-21G(d)] basis sets. For pseudopotential calculations, the Stuttgart[15,16] ECPs and corresponding basis sets were used on heavy atoms according to the defaults in the Gaussian 03 software. For the elements relevant to this study, the ECPs are MWB10 (Al−Cl, Zn), MDF10 (Ti), MWB28 (Ga−Br), and MWB46 (I), where "MWB" and "MDF" denote quasi-relativistic and relativistic ECPs, respectively, and the numerical suffix indicates the number of core electrons replaced by the effective potential. A set of *d* polarization functions, taken from the corresponding 6-311G(d,p) [3-21G(d)] all-electron basis, was added to each heavy center. The combination of ECP, basis, and polarization set is labeled ECP(d) here.

The BEB ionization cross section is sensitive to the vertical ionization energy of the molecule, that is, the ionization threshold. Koopmans (i.e., Hartree−Fock) binding energies are too approximate for this purpose. More accurate values of B for the valence orbitals were computed using the outer-valence Green's function (OVGF) method[17,18] with the 6-311+G(d,p) [3-21G(d)] basis sets. For the chlorofluoromethanes, the binding energies from this procedure are lower than corresponding experimental values by only 0.3 eV.[1] OVGF results were rejected for pole strengths < 0.75. When available, experimental vertical ionization energies were used for the outermost valence orbitals. Second ionization energies, IE_2, were taken either from experiment or from B3LYP/6-311G(d,p) [ECP(d)] calculations at the geometry of the neutral molecule, considering both singlet and triplet dications. Mulliken populations for each MO were generated by using the program MullPop,[19] which was kindly modified by its author to accommodate Gaussian 03 output files.

At low impact energies, the core orbitals make only a small contribution to the ionization cross section and can be neglected. Thus, if one is interested only in low energies, ECP calculations alone are adequate for computing ionization cross sections. For such calculations, geometries were optimized at the B3LYP/6-31G(d,p) [ECP(d)] level.

Table 1. Experimental Ionization Energies Used in BEB Calculations[e]

molecule	IE_v[a] (eV)	IE_2[b] (eV)
C_2Cl_6	$2a_{2g} = 11.22$, $9e_g = 11.37$, $2a_{1u} = 11.79$;[48] (11.02, 11.17, 11.52)	28.8 ± 0.5[49] (26.3)
C_2HCl_5	$20a'' = 11.28$, $19a'' = 29a' = 11.56$, $28a' = 18a'' = 12.09$;[48] (10.98, 11.28, 11.45, 11.79, 11.74)	28.7 ± 0.5[49] (26.4)
C_2Cl_4	$3b_{3u} = 9.51$, $7b_{3g} = 11.37$, $2a_u = 7b_{2u} = 12.19$, $2b_{1g} = 8b_{1u} = 9a_g = 12.58$;[48] (9.59, 11.13, 11.94, 12.11, 12.26, 12.43, 12.73)	
1,1,1,2-$C_2H_2Cl_4$	$14a'' = 11.45$, $27a' = 13a'' = 11.67$, $12a'' = 26a' = 11.91$, $25a' = 12.37$, $24a' = 11a'' = 12.83$;[48] (11.13, 11.30, 11.32, 11.57, 11.67, 12.04, 12.50, 12.55)	28.2 ± 0.5[49] (26.8)
1,1,2,2-$C_2H_2Cl_4$	$9b_g = 11.17$, $12a_g = 9a_u = 11.62$;[48] (10.84, 11.34, 11.56)	28.7 ± 0.5[49] (26.8)
CCl_4	$2t_1 = 11.69$, $7t_2 = 12.62$, $2e = 13.44$;[48] (11.39, 12.31, 13.03)	29.1 ± 0.1[50] (28.0)
$TiCl_4$	$2t_1 = 11.69$, $9t_2 = 12.67$, $2e = 13.17$, $8t_2 = 13.46$;[51] (11.69, 12.94, 13.41, 14.12)	
CBr_4	$5t_1 = 10.39$, $13t_2 = 11.07$, $5e = 12.11$;[52] (10.27, 11.12, 11.82)	
$CHBr_3$	$5a_2 = 10.5$, $18e = 10.8$, $15a_1 = 11.3$, $17e = 11.7$;[52] (10.18, 10.65, 10.83, 11.38)	27.9 ± 0.2[53] (26.2)
CH_2Br_2	$13b_2 = 10.6$, $6b_1 = 10.8$, $5a_2 = 15a_1 = 11.3$;[52] (10.28, 10.47, 10.76, 10.90)	27.4 ± 0.2[53] (27.0)
P_2	$2\pi_u = 10.62$, $5\sigma_g = 10.81$;[54] (10.49, 10.71)	
P_4	$2e = 9.46$, 9.92;[c] $6t_2 = 10.36$, 10.53, 10.72;[c] $5a_1 = 11.85$;[55] (9.53, 10.29, 11.70)	
As_2	$4\pi_u = 9.82$, 9.96;[d] $8\sigma_g = 10.22$;[56] (9.75, 10.13)	
As_4	$5e = 8.75$, 9.16;[c] $12t_2 = 9.76$, 9.97, 10.11;[c] $8a_1 = 11.06$;[55] (8.84, 9.76, 10.94)	
GaCl	$12\sigma_g = 10.07$, $5\pi = 11.38$;[36] (9.55, 10.93)	
CS_2	$2\pi_g = 10.06$, $2\pi_u = 12.83$;[48] (9.79, 13.12)	27.22 ± 0.08[57] (27.0)
H_2S	$2b_1 = 10.48$, $5a_1 = 13.25$;[48] (9.87, 12.95)	32.8[58] (31.9)
CH_3I	$9e = 9.54$, 10.16;[d] $13a_1 = 12.50$;[48] (9.15, 12.07)	
$Al(CH_3)_3$	$5e' = 9.85$, $6a' = 12.6$;[59] (9.71, 12.84)	
$Ga(CH_3)_3$	$7e' = 9.76$, $8a' = 13.5$;[60,61] (9.54, 13.16)	
TMS_2O	$16a_1 = 8b_1 = 9.88$, $14b_2 = 7a_2 = 10.73$, $15a_1 = 7b_1 = 12.5$;[62] (9.77, 9.79, 10.59, 10.59, 12.31, 12.31)	
$Zn(C_2H_5)_2$	$15b = 8.6$, $17a = 10.5$;[63] (8.53, 10.28)	

[a] Vertical ionization energy. [b] Double-ionization energy. [c] Jahn−Teller split. [d] Spin−orbit split. [e] Calculated OVGF values listed parenthetically, for comparison. All values in eV.

The series of computations were performed automatically by means of a Perl-language script. The output of this script is a summary of the MO data in the tab-delimited format used in the NIST database.[4] This file serves as input to another Perl script, which computes energy-dependent cross sections.

Electric dipole polarizabilities, which are not part of the BEB procedure but are relevant in the Results section, were computed using the Gaussian 03 and GAMESS programs as convenient.[12,20]

Results

We selected several molecules for which total ionization cross sections have been measured experimentally and which contain as many heavy atoms as possible yet which do not contain atoms so heavy that all-electron basis sets are unavailable. This set of molecules was intended to accentuate differences between the all-electron and ECP predictions. For computational convenience, only closed-shell molecules were considered. Along with literature references for the experimental cross sections, the molecules are as follows: C_2Cl_6, C_2HCl_5, C_2Cl_4, 1,1,1,2-$C_2H_2Cl_4$, and 1,1,2,2-$C_2H_2Cl_4$;[7] CCl_4;[7,21,22] $TiCl_4$;[23] CBr_4, $CHBr_3$, and CH_2Br_2;[6] P_2, P_4, As_2, and As_4;[24] GaCl;[25] CS_2;[26−28] H_2S;[27,29,30] CH_3I;[5,31] $Al(CH_3)_3$ and $Ga(CH_3)_3$;[32] hexamethyldisiloxane (TMS_2O);[33] $Zn(C_2H_5)_2$.[34]

Tables of MO data used to generate the BEB cross sections are available as Supporting Information. As mentioned above, some vertical ionization energies and double-ionization energies were taken from experimental measurements. These experimental values are listed in Table 1 with their sources. The corresponding calculated values are listed parenthetically for comparison. In some cases, the theoretical results led us to reassign the experimental photoelectron spectra.

Ionization cross sections are used for a variety of applications, suggesting a variety of criteria for comparing theoretical predictions with experimental measurements. We consider four criteria in this study:

(1) Peak cross section: The difference between theory and experiment may be expressed in absolute terms ($Å^2$) or as a percentage of the experimental value.

(2) Cross section at energy of maximum difference between AE and ECP predictions: This is the energy at which the two models are most easily distinguished. The difference between theory and experiment may be expressed in absolute terms ($Å^2$) or as a percentage of the experimental value.

(3) Shape of the cross-section curve, plotted as a function of incident electron energy: Predicting the shape of the curve is most useful when reliable experimental measurements are only available at a few impact energies.[35]

(4) Initial slope: The energy dependence of the cross section at low energies is important for plasma modeling. The difference between theory and experiment may be expressed in absolute terms ($Å^2$/eV) or as a percentage of the experimental value.

Peak Cross Section. The simplest comparison between theoretical and experimental cross sections is simply the peak value. Table 2 lists the peak cross sections from experimental measurements and from BEB calculations using both all-electron (AE) and ECP approaches. The effect of changing the Mulliken population threshold is addressed below; the

Table 2. Experimental and Calculated Peak Total Ionization Cross Sections in Å^2 (1 Å^2 = 10^{-20} m^2)[c]

molecule	expt	BEB-AE	BEB-ECP
C_2Cl_6	26.61 ± 1.06[7]	25.9	24.7
C_2HCl_5	23.61 ± 0.94[7]	22.7	21.6
C_2Cl_4	21.74 ± 0.87[7]	18.0	17.8
1,1,1,2-$C_2H_2Cl_4$	21.24 ± 0.85[7]	19.1	18.4
1,1,2,2-$C_2H_2Cl_4$	19.66 ± 0.79[7]	19.6	18.8
CCl_4	15.45 ± 0.62[7]	16.4	15.6
	15.15 ± 0.76[21]		
	14.9 ± 1.5[22]		
$TiCl_4$	16.45 ± 2.47[23]	19.9	17.5
CBr_4	19.0 ± 0.76[6]	20.6	19.7
$CHBr_3$	13.75 ± 0.55[6]	15.4	14.9
CH_2Br_2	11.67 ± 0.47[6]	11.5	11.4
P_2	9.0 ± 1.4[24]	8.5	7.6
P_4	21.0 ± 3.4[24]	17.0	15.1
As_2	13.2 ± 2.1[24]	9.7	8.6
As_4	27.2 ± 4.3[24]	19.4	17.1
GaCl	9.25 ± 0.93[25]	8.6	8.3
CS_2	9.03 ± 0.54[27]	9.7	9.4
	11.70 ± 0.47[28]		
	8.85 ± 1.33[26]		
H_2S	3.93 ± 0.51[30]	4.9	4.6
	5.53 ± 0.33[27]		
	6.28[29]		
CH_3I	10.3 ± 0.3[5]	8.9	8.7
	9.64 ± 0.58[31]		
$Al(CH_3)_3$	13 ± 1[32] [a]	14.0[a]	14.4[a]
$Ga(CH_3)_3$	12 ± 1[32] [a]	14.1[a]	14.9[a]
TMS_2O	26.41 ± 3.96[33] [b]	28.0[b]	28.6[b]
$Zn(C_2H_5)_2$	7.9 ± 1.4[34]	17.1	17.6

[a] At 70 eV, not necessarily the peak. [b] At 100 eV, not necessarily the peak. [c] A Mulliken population threshold of 75% was used in the AE calculations.

AE values in Table 2 were computed using a threshold of 75%, which we denote AE75. The differences between the calculated and experimental peak cross sections are plotted in Figure 1. Anomalously large discrepancies are apparent for $Zn(C_2H_5)_2$ and for As_4. These anomalies and questions about these experiments, described below, lead us to exclude from primary consideration the five molecules [P_2, P_4, As_2, As_4, $Zn(C_2H_5)_2$] measured in these two experiments.

From Table 2, the average reported experimental uncertainty is 1.2 Å^2. Excluding the five molecules mentioned above, the average reported experimental uncertainty is 0.9 Å^2, and the mean deviations from experimental values are 0.1 and −0.3 Å^2 for the AE75 and ECP approaches, respectively. The standard deviations of the discrepancies are 1.6 Å^2 for both AE75 and ECP methods. On average, the peak cross sections from AE75 calculations are 0.5 Å^2 larger than from ECP calculations (standard deviation = 0.6 Å^2).

The discrepancies in Table 2 may also be considered on a fractional basis. The mean reported experimental uncertainty is then 8%. When the same five molecules are excluded as above, the mean experimental uncertainty is 7%, and the mean deviations from the experimental values are 1% and −2% for the AE75 and ECP methods, respectively, both with standard deviation of 13%, all as percentages of the experimental values. On average, the peak cross sections from AE75 calculations are 4% larger than from ECP calculations (standard deviation = 4%). As expected, the fractional discrepancy between the AE and ECP predictions is greatest at low electron energy, where the cross section has a small value. For example, the AE75 prediction exceeds the ECP prediction for C_2Cl_6 by 31% at 15 eV, 5% at 70 eV, and 1% at 200 eV.

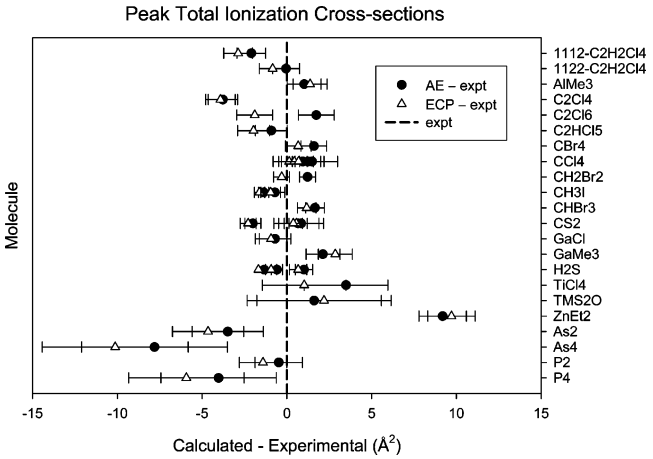

Figure 1. Differences between theoretical peak cross sections (both all-electron and effective-core-potential calculations) and experimental peak cross sections for 22 molecules. A Mulliken population threshold of 75% was used in the all-electron calculations. Error bars indicate the reported experimental uncertainties. A difference of zero corresponds to perfect agreement between theory and experiment.

Cross Section at Energy of Maximum Difference. The absolute difference between the AE and ECP predictions is greatest somewhat below the peak in the cross section. For example, the AE75 prediction exceeds the ECP prediction for C_2Cl_6 by 1.0 Å^2 at 15 eV, 2.1 Å^2 at 40 eV, 1.2 Å^2 at 70 eV, and 0.2 Å^2 at 200 eV. This suggests that the AE and ECP predictions are best compared not at the peak in the cross section, as in Table 2, but at some lower energy, where their contrast is greatest. Table 3 lists cross sections at energies where the difference between the AE75 and ECP predictions is greatest. Experimental values are included when available. Excluding the same five molecules as before, the mean deviations from experimental values are 0.8 and −0.1 Å^2 for the AE75 and ECP approaches, respectively. As fractions of the experimental values, the respective mean deviations are 10% and −1% for the AE75 and ECP methods.

Shape of the Cross-Section Curve. There is no standard procedure for comparing experimental and theoretical curve shapes. Here we use the minimized root-mean-square difference (rmsd) given by eq 2, where the integral is over the range of the experimental data and the scaling parameter s is chosen to minimize rmsd for each data set individually.

$$\mathrm{rmsd} = [(T_{\max} - T_{\min})^{-1} \int_{T_{\min}}^{T_{\max}} (s\sigma_{\mathrm{BEB}} - \sigma_{\mathrm{expt}})^2 \mathrm{d}T]^{1/2} \quad (2)$$

The values of rmsd (and s) for each experimental data set are listed in Table 4. Excluding the same five molecules as before, the average values of rmsd are 0.8 and 0.6 Å^2 for

Table 3. Experimental and Calculated Total Ionization Cross Sections at Energies Where AE and ECP Predictions Differ Most[a]

molecule	energy	expt	AE75	ECP
C_2Cl_6	28	15.3 ± 0.6[7]	17.7	15.4
C_2HCl_5	26	13.0 ± 0.5[7]	14.2	12.3
C_2Cl_4	24	11.6 ± 0.5[7]	9.9	9.1
1,1,1,2-$C_2H_2Cl_4$	26	12.4 ± 0.5[7]	11.8	10.3
1,1,2,2-$C_2H_2Cl_4$	26	11.6 ± 0.5[7]	12.4	10.8
CCl_4	28	9.6 ± 0.4[7]	10.9	9.5
		9.0 ± 0.4[21]		
		11.4 ± 1.1[22]		
$TiCl_4$	38	14.9 ± 2.2[23]	17.6	14.5
CBr_4	23.5		13.4	11.5
$CHBr_3$	23	6.5 ± 0.3[6]	9.9	8.6
CH_2Br_2	21.5	5.2 ± 0.2[6]	6.6	5.7
P_2	30	5.3 ± 0.8[24]	7.6	6.4
P_4	30	15.7 ± 2.5[24]	14.8	12.5
As_2	28	3.4 ± 0.5[24]	8.7	7.2
As_4	28	14.2 ± 2.3[24]	17.1	14.2
GaCl	23	7.9 ± 0.8[25]	5.3	4.6
CS_2	30	6.9 ± 0.4[27]	7.8	7.1
		6.4 ± 0.3[28]		
		8.7 ± 1.3[26]		
H_2S	30	3.3 ± 0.4[30]	4.0	3.5
		5.1 ± 0.3[27]		
		5.1[29]		
CH_3I	19.5	3.4 ± 0.1[31]	4.8	4.3
$Al(CH_3)_3$	34	8.9 ± 0.7[32]	11.2	11.6
$Ga(CH_3)_3$	38	9.7 ± 1.0[32]	11.2	12.1
TMS_2O	40	22.3 ± 3.3[33]	24.5	25.4
$Zn(C_2H_5)_2$	50	7.3 ± 1.3[34]	16.0	16.6

[a] Energies in eV, cross sections in Å^2. A Mulliken population threshold of 75% was used in the AE calculations.

the AE75 and ECP approaches, respectively. On average, the ECP value is 15% smaller than the AE75 value.

Initial Slope. Cross-section curves are not linear. The initial slope is defined here as the slope of the least-squares line through the experimental set of low-energy data points, i.e., from the threshold up to twice the threshold energy. These same low energies are used to compute theoretical cross sections, which are then fitted with a line to determine the corresponding theoretical initial slope. Results are collected in Table 5. Excluding the same five molecules as before, the average discrepancies with experimental values are −0.1 and −0.5 Å^2/eV for the AE75 and ECP methods, respectively. As fractions of the experimental values, the respective mean deviations are 2% and −6% for the AE75 and ECP methods. For the molecule GaCl, the experimental ionization threshold (6 eV) is much lower than the molecular ionization energy (10.07 eV).[36] The authors attributed this to ion pair formation, $Ga^+ + Cl^-$ (although the threshold is 1.4 eV too low),[25] which is not included in the BEB theory. Another possibility is unwanted, atomic Ga (IE = 5.9993 eV)[37] formed during the ion neutralization process. Thus, GaCl data points below 10 eV were omitted from our analysis.

Statistics for all the comparisons are collected in Table 6. For the AE calculations, results are tabulated for Mulliken population thresholds of 25%, 50%, 75%, and 85% as relevant to the choice of n in eq 1. The upper part of Table 6 excludes the five questionable molecules. The lower part of Table 6 includes all molecules. Differences between theory and experiment are listed in both absolute and fractional (percentage) terms. Since a small mean difference can conceal large discrepancies, root-mean-square (rms) differences are also listed. For all entries in Table 6, a value of zero corresponds to ideal agreement between theory and experiment.

Table 4. Comparison of the Shapes of the Experimental and Calculated Cross-Section Curves[a]

	rmsd (Å^2)		fitting parameter s	
molecule	AE75	ECP	AE75	ECP
C_2Cl_6[7]	2.06	1.04	0.97	1.09
C_2HCl_5[7]	1.50	0.65	1.01	1.11
C_2Cl_4[7]	1.03	0.30	1.10	1.23
1,1,1,2-$C_2H_2Cl_4$[7]	0.97	0.38	1.07	1.17
1,1,2,2-$C_2H_2Cl_4$[7]	1.00	0.39	0.97	1.06
CCl_4[7,21,22]	0.51	0.21	0.88	0.98
	0.99	0.55	0.97	1.05
	0.79	1.22	0.87	1.01
$TiCl_4$[23]	0.37	0.66	0.83	0.90
$CHBr_3$[6]	1.19	0.68	0.85	0.93
CH_2Br_2[6]	0.75	0.31	0.93	1.02
P_2[24]	1.85	1.51	1.15	1.29
P_4[24]	3.64	3.06	1.45	1.61
As_2[24]	4.19	3.72	1.26	1.42
As_4[24]	5.41	4.23	1.55	1.72
GaCl[25]	0.85	1.12	1.00	1.07
CS_2[26−28]	0.80,	0.60	0.95	1.03
	0.44	0.20	0.92	1.00
	1.73	1.22	1.13	1.28
H_2S[27,29,30]	0.16,	0.17	1.18	1.23
	0.15	0.12	1.27	1.37
	0.73	0.68	1.04	1.08
CH_3I[31]	0.53	0.28	1.10	1.16
$Al(CH_3)_3$[32]	0.47	0.51	0.84	0.81
$Ga(CH_3)_3$[32]	0.80	0.66	0.86	0.81
TMS_2O[33]	1.64	1.57	0.91	0.89
$Zn(C_2H_5)_2$[34]	0.23	0.25	0.45	0.44

[a] A better match yields a smaller value of rmsd from eq 2. A Mulliken population threshold of 75% was used in the AE calculations.

Comments on Experimental Measurements for P_2, P_4, As_2, and As_4. The experimental results for As_2, As_4, P_4, and P_2 were reported in the same paper.[24] All were measured using a Knudsen cell. Different precursors were required for the tetramers and the dimers. The number densities of the neutral gases were inferred from the rate of mass flow and the equations describing molecular flow. A multiplicative instrumental correction factor was derived from room-temperature measurements of N_2 and Ar. We suggest that the number densities estimated by this procedure were somewhat too low.

Comments on Experimental Measurements for $Zn(C_2H_5)_2$. In the $Zn(C_2H_5)_2$ experiment,[34] it was assumed that the Ar:$Zn(C_2H_5)_2$ pressure ratio in the gas reservoir was retained in the mass spectrometer. This neglects the expected mass discrimination in the leak valve, which depends on the molecular masses as $(M_{Zn(C_2H_5)_2}/M_{Ar})^{1/2} \approx 1.76$.[38] Applying this correction raises the peak experimental cross section to 13.9 ± 2.5 Å^2, much closer to the theoretical values.

Table 5. Experimental and Calculated Initial Slopes (Å²/eV) of Total Ionization Cross-Section Curves, as Defined in the Text[b]

molecule	expt	AE75	ECP
C_2Cl_6	0.95[7]	0.91	0.85
C_2HCl_5	0.86[7]	0.78	0.74
C_2Cl_4	0.81[7]	0.61	0.60
1,1,1,2-$C_2H_2Cl_4$	0.86[7]	0.77	0.71
1,1,2,2-$C_2H_2Cl_4$	0.77[7]	0.68	0.65
CCl_4	0.50,[7] 0.57[21], 0.77[22]	0.76	0.65
$TiCl_4$	0.76[23]	1.05	0.81
$CHBr_3$	0.50[6]	0.78	0.70
CH_2Br_2	0.44[6]	0.58	0.53
P_2	0.37[24]	0.32	0.28
P_4	1.09[24]	0.59	0.52
As_2	0.24[24]	0.33	0.30
As_4	0.99[24]	0.62	0.56
GaCl[a]	0.63[25]	0.48	0.42
CS_2	0.48,[27] 0.34,[28] 0.61[26]	0.51	0.46
H_2S	0.17,[30] 0.20,[27] 0.32[29]	0.19	0.18
CH_3I	0.38[31]	0.40	0.39
$Al(CH_3)_3$	0.60[32]	0.61	0.64
$Ga(CH_3)_3$	0.66[32]	0.50	0.57
TMS_2O	1.36[33]	1.06	1.12
$Zn(C_2H_5)_2$	0.23[34]	0.69	0.71

[a] Points deleted below thermodynamic threshold. [b] A Mulliken population threshold of 75% was used in the AE calculations.

Mixing between the heavy and light gases in the reservoir may also have been incomplete, which would reduce the proportion of the zinc compound if gas were withdrawn from the upper part of the reservoir, further underestimating the ionization cross section.

Mass discrimination is often problematic in Fourier transform mass spectrometry (FTMS).[39] Most seriously, FTMS suffers from a low-mass cutoff; it fails to detect ions with cyclotron frequencies too high (that is, masses too low) for the analog-to-digital converter. Although remedies have been developed,[40−42] they have not become popular. No ions lighter than C_2H^+ were reported in either of the FTMS studies cited here.[32,34] This suggests the possibility that the total ion yields were underestimated.

Reaction rate constants provide another way to determine pressure inside an FTMS cell. The authors made the reasonable assumption that charge transfer with Ar^+ occurs at the collision rate. The second-order collision rate constant can be computed from ion−molecule collision theory and combined with the pseudo-first-order rate constant for charge transfer to deduce the pressure of $Zn(C_2H_5)_2$. For this purpose, we calculate the isotropic polarizability of $Zn(C_2H_5)_2$ to be $\alpha = 11.38$ Å^3 (and dipole moment $\mu_D = 5.2 \times 10^{-31}$ Cm = 0.16 D) at the MP2/6-311++G(3d2f,3p2d) level, using a B3LYP/6-31G(d) geometry. Analogous calculations for Zn atom, C_2H_6, and CH_4 yield $\alpha = 5.64$, 4.20, and 2.43 Å^3, respectively, which are lower than the corresponding experimental values,[43] 5.75, 4.47, and 2.593 Å^3, by approximately 0.14 Å^3 per non-hydrogen atom. After applying this correction, our predicted polarizability for $Zn(C_2H_5)_2$ is 12.1 Å^3, which corresponds to a collision rate with Ar^+ of 1.5×10^{-9} cm^3 molecule^{-1} s^{-1}, according to the average dipole orientation[44] (ADO) theory. Unfortunately, since the pseudo-first-order rate constant was not reported, we cannot infer the pressure of $Zn(C_2H_5)_2$ in the FTMS experiment.

Table 6. Differences between Theory and Experiment: Summary Statistics and Effects of Varying the Mulliken Population Threshold[a]

comparison with expt	ECP	AE25	AE50	AE75	AE85
Five Molecules [P_2, P_4, As_2, As_4, $Zn(C_2H_5)_2$] Excluded					
peak: mean (Å²)	−0.3	1.2	1.1	*0.1*	−0.2
peak: mean %	−2%	8%	8%	*1%*	−3%
peak: rms (Å²)	**1.6**	1.9	1.9	*1.6*	1.8
peak: rms %	**12%**	15%	15%	*12%*	14%
max|AE-ECP|: AE mean (Å²)		1.7	1.6	0.8	*0.4*
max|AE-ECP|: ECP mean (Å²)		−0.2	−0.2	−0.1	**0.0**
max|AE-ECP|: AE mean %		14%	14%	10%	*6%*
max|AE-ECP|: ECP mean %		−2%	−2%	−1%	**1%**
max|AE-ECP|: AE rms (Å²)		2.3	2.3	*1.7*	1.8
max|AE-ECP|: ECP rms (Å²)		1.7	1.7	**1.7**	1.6
max|AE-ECP|: AE rms %		*22%*	*22%*	23%	23%
max|AE-ECP|: ECP rms %		**17%**	**17%**	20%	18%
shape [eq 2]: mean (Å²)	**0.61**	0.89	0.88	0.75	*0.72*
initial slope: mean (Å²/eV)	−0.05	0.05	0.05	*−0.01*	−0.03
initial slope: mean %	−6%	11%	11%	*2%*	−3%
initial slope: rms (Å²/eV)	**0.12**	0.16	0.16	*0.15*	0.16
initial slope: rms %	**19%**	29%	28%	*23%*	26%
All Molecules Included					
peak: mean (Å²)	−0.7	0.8	0.7	*−0.1*	−0.4
peak: mean %	−2%	8%	8%	2%	*−1%*
peak: rms (Å²)	3.3	3.0	3.0	*2.9*	*2.9*
peak: rms %	28%	27%	27%	*26%*	*26%*
max|AE-ECP|: AE mean (Å²)		2.0	1.9	1.3	*1.0*
max|AE-ECP|: ECP mean (Å²)		0.2	0.2	0.3	**0.4**
max|AE-ECP|: AE mean %		24%	24%	20%	*17%*
max|AE-ECP|: ECP mean %		8%	8%	8%	**10%**
max|AE-ECP|: AE rms (Å²)		2.8	2.8	*2.6*	2.7
max|AE-ECP|: ECP rms (Å²)		2.4	2.4	**2.5**	2.5
max|AE-ECP|: AE rms %		44%	44%	44%	44%
max|AE-ECP|: ECP rms %		**37%**	**37%**	**38%**	**37%**
shape [eq 2]: mean (Å²)	**0.97**	1.29	1.29	1.18	*1.16*
initial slope: mean (Å²/eV)	−0.06	0.03	*0.02*	*−0.02*	−0.04
initial slope: mean %	**−1%**	14%	14%	7%	*3%*
initial slope: rms (Å²/eV)	**0.20**	0.21	0.21	*0.20*	0.21
initial slope rms %	**46%**	48%	48%	*46%*	47%

[a] E.g., AE85 denotes AE calculations using a threshold of 85%. See the Discussion section for the meaning of the italic and bold fonts.

Discussion

Some published BEB calculations have incorrectly computed the parameter n from eq 1. As discussed elsewhere,[45] this has led to inaccurately unfavorable characterizations of the reliability of BEB theory for molecules containing the heavier elements ($Z > 10$). The present calculations are compared with experimental measurements for CCl_4, C_2Cl_6, and CS_2 in Figures 2-4. These figures exemplify the performance of BEB theory for molecules containing 3p elements such as chlorine and sulfur.

Although the reported experimental uncertainties are small, the disparity among measurements suggests that the total experimental uncertainty, including bias, may exceed 20%.[1] For example, multiple experimental measurements are available for CCl_4 (three measurements), CS_2 (three), H_2S (three),

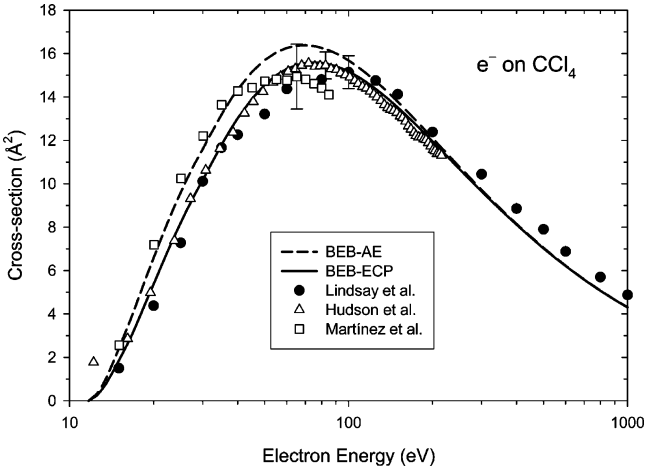

Figure 2. Total ionization cross section for CCl_4. Theoretical values are indicated by the solid (effective core-potential) and dashed (all-electron) curves. Experimental values are indicated by the symbols.[7,21,22]

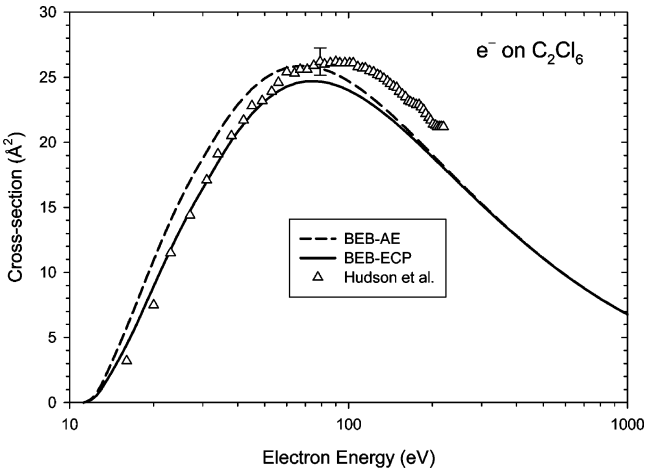

Figure 3. Total ionization cross section for C_2Cl_6. Theoretical values are indicated by the solid (effective core-potential) and dashed (all-electron) curves. Experimental values are indicated by the symbols.[7]

and CH_3I (two) (Table 2), with peak cross sections spanning 4%, 29%, 45%, and 7% of the respective mean values. Thus, the cross sections from both the all-electron (AE) and effective-core-potential (ECP) calculations agree with experimental measurements as well as different experimental measurements agree with each other. As judged from Tables 2−6 and the figures, differences between the AE the ECP predictions are generally minor.

Table 6 summarizes quantitatively the agreement with experiment that is achieved by both the AE and ECP implementations of BEB theory. We exclude the five problematic molecules from this discussion (top half of Table 6). The effects of including them, shown in the bottom half of Table 6, are minor.

Mulliken Population Threshold in AE Calculations. For each row in Table 6, values in italics indicate which value of the Mulliken population threshold (in the AE calculations) agrees best with the available experimental data. The first four rows refer to the peak value of the ionization cross section. All four agree best when the Mulliken population threshold is 75%.

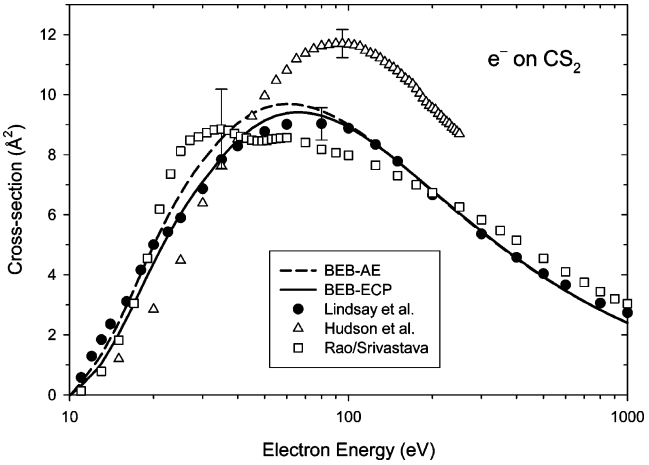

Figure 4. Total ionization cross section for CS_2. Theoretical values are indicated by the solid (effective core-potential) and dashed (all-electron) curves. Experimental values are indicated by the symbols.[26−28]

The next eight rows refer to the impact energy that maximizes the absolute difference between the AE and ECP predictions. This energy is generally different for each molecule. Considering only the mean discrepancies with experiment at these energies, the best Mulliken population threshold appears to be 85%. However, small mean values can mask large positive and negative discrepancies that happen to counterbalance each other. If absolute root-mean-square (rms) discrepancies with experimental values are considered instead, the best threshold appears to be 75%. Relative rms discrepancies weakly favor a lower threshold of 50% or 25%.

The non-negative shape comparison [eq 2] favors a Mulliken population threshold of 85%. The last four rows of the top half of Table 6, all dealing with the initial slope of the cross-section curve, all favor a threshold of 75%. Considering all rows of the top half of Table 6, the best choice of Mulliken population threshold appears to be 75%.

ECP vs AE Calculations. In Table 6, results of ECP calculations are shown in boldface when they agree with experiment at least as well as the best AE results. For peak cross sections, the AE mean value is slightly better than the ECP mean value. The ECP and AE peak values are equally good on an rms basis.

At the energies where the ECP and AE predictions differ most, the ECP mean value agrees with experiment better than the AE value does. The ECP results are slightly better than the AE results on an rms basis.

The shapes of the ECP curves agree better with experimental data than do the AE results, as measured using eq 2. On an averaged basis, the AE initial slopes agree with experiment better than the ECP slopes do. However, the order is reversed when the slopes are compared on an rms basis. Considering all the data of Table 6, the ECP predictions agree better with experimental measurement by some metrics and the AE predictions agree better by other metrics. Overall, the ECP predictions agree better with experiment, although the AE calculations agree nearly as well.

The ECP approach has operational advantages over the AE method. The ECP procedure is more clearly defined. In the AE procedure, one must use Mulliken populations to identify valence orbitals that are dominated by atomic orbitals with principal quantum number n greater than 2. The Mulliken population threshold for identifying such molecular orbitals, although recommended here as 75%, is rather arbitrary. There is further ambiguity when multiple heavy atoms are involved. For example, in the molecule MoO_2Cl_2 (not included in the Tables), orbital $10b_1$ has 38% Mo 4d character and 24% Cl 3p character; the appropriate value of n in eq 1 is debatable. In contrast, no Mulliken populations are needed in the ECP approach.

The ECP method is more easily extensible to molecules containing very heavy atoms, for which good all-electron basis sets are often unavailable. As a bonus, many ECPs also recover scalar relativistic effects, thus providing more accurate energies. We find that the results are independent of the choice of effective potential. For example, the Stuttgart,[15,16] NIST,[46] and Los Alamos[47] ECPs, with their corresponding valence basis sets, produce nearly superimposable cross-section curves for C_2Cl_4 (differences less than 0.1 Å^2).

The ECP procedure still requires performing all-electron calculations to obtain cross sections for the core orbitals. This is cumbersome for molecules containing very heavy atoms that lack good all-electron basis sets. Alternatively, binding and kinetic energies for the core orbitals can be obtained from atomic Dirac−Fock calculations,[9] independent of the particular molecule at hand. For the molecules examined here, completely ignoring the contribution of the core by using ECPs for all calculations reduces the cross section by only a small percentage, particularly at energies below 100 eV. Thus, the core can be neglected entirely if the energies of interest are not too high. This is the situation in applications such as mass spectrometry or low-energy plasmas.

Conclusions

Both the all-electron (AE) and effective-core-potential (ECP) implementations of the BEB theory produce total ionization cross sections that agree with experimental measurements about as well as different experiments agree with each other. The ECP predictions show slightly better agreement with experimental measurements, as evaluated using a variety of metrics. The ECP method is also more convenient, since it avoids Mulliken population thresholds, is applicable to larger molecules and heavier atoms, carries a lower computational cost, and includes scalar relativistic effects. We recommend the ECP approach for calculating BEB cross sections for molecules that contain elements heavier than neon.

Acknowledgment. We are grateful to Prof. Reinaldo Pis Diez (Universidad Nacional de La Plata) for providing and modifying the MullPop program and to Dr. Yong-Ki Kim (NIST) for general encouragement and for pointing out the importance of the shape of the cross-sections curves. We also thank the referees for their comments, especially for suggesting that the Mulliken population threshold be considered as an adjustable parameter and that the initial slope is an interesting quantity. G.E.S. is a NIST Summer Undergraduate Research Fellow, 2003.

Supporting Information Available: Molecular orbital data for the 22 molecules listed in the tables, as obtained by using the AE25, AE50, AE75, AE85, and ECP methods (110 ASCII files). This material is available free of charge via the Internet at http://pubs.acs.org.

References

(1) Irikura, K. K.; Ali, M. A.; Kim, Y.-K. *Int. J. Mass Spectrom.* **2003**, *222*, 189−200.

(2) Kim, Y.-K.; Rudd, M. E. *Phys. Rev. A* **1994**, *50*, 3954−3967.

(3) Hwang, W.; Kim, Y.-K.; Rudd, M. E. *J. Chem. Phys.* **1996**, *104*, 2956−2966.

(4) Kim, Y.-K.; Irikura, K. K.; Rudd, M. E.; Zucker, D. S.; Zucker, M. A.; Coursey, J. S.; Olsen, K. J.; Wiersma, G. G. *Electron-Impact Ionization Cross Section Database* (vers. 2.1); National Institute of Standards and Technology, Gaithersburg, MD: http://physics.nist.gov/ionxsec.

(5) Vallance, C.; Harris, S. A.; Hudson, J. E.; Harland, P. W. *J. Phys. B: At., Mol. Opt. Phys.* **1997**, *30*, 2465−2475.

(6) Bart, M.; Harland, P. W.; Hudson, J. E.; Vallance, C. *Phys. Chem. Chem. Phys.* **2001**, *3*, 800−806.

(7) Hudson, J. E.; Vallance, C.; Bart, M.; Harland, P. W. *J. Phys. B: At., Mol. Opt. Phys.* **2001**, *34*, 3025−3039.

(8) Kim, Y.-K.; Hwang, W.; Weinberger, N. M.; Ali, M. A.; Rudd, M. E. *J. Chem. Phys.* **1997**, *106*, 1026−1033.

(9) Huo, W. M.; Kim, Y.-K. *Chem. Phys. Lett.* **2000**, *319*, 576−586.

(10) Berry, R. S.; Rice, S. A.; Ross, J. *Physical Chemistry*; John Wiley & Sons: New York, 1980.

(11) Certain commercial materials and equipment are identified in this paper in order to specify procedures completely. In no case does such identification imply recommendation or endorsement by the National Institute of Standards and Technology, nor does it imply that the material or equipment identified is necessarily the best available for the purpose.

(12) Frisch, M. J.; Trucks, G. W.; Schlegel, H. B.; Scuseria, G. E.; Robb, M. A.; Cheeseman, J. R.; Montgomery, J. A., Jr.; Vreven, T.; Kudin, K. N.; Burant, J. C.; Millam, J. M.; Iyengar, S. S.; Tomasi, J.; Barone, V.; Mennucci, B.; Cossi, M.; Scalmani, G.; Rega, N.; Petersson, G. A.; Nakatsuji, H.; Hada, M.; Ehara, M.; Toyota, K.; Fukuda, R.; Hasegawa, J.; Ishida, M.; Nakajima, T.; Honda, Y.; Kitao, O.; Nakai, H.; Klene, M.; Li, X.; Knox, J. E.; Hratchian, H. P.; Cross, J. B.; Adamo, C.; Jaramillo, J.; Gomperts, R.; Stratmann, R. E.; Yazyev, O.; Austin, A. J.; Cammi, R.; Pomelli, C.; Ochterski, J. W.; Ayala, P. Y.; Morokuma, K.; Voth, G. A.; Salvador, P.; Dannenberg, J. J.; Zakrzewski, V. G.; Dapprich, S.; Daniels, A. D.; Strain, M. C.; Farkas, O.; Malick, D. K.; Rabuck, A. D.; Raghavachari, K.; Foresman, J. B.; Ortiz, J. V.; Cui, Q.; Baboul, A. G.; Clifford, S.; Cioslowski, J.; Stefanov, B. B.; Liu, G.; Liashenko, A.; Piskorz, P.; Komaromi, I.; Martin, R. L.; Fox, D. J.; Keith, T.; Al-Laham, M. A.; Peng, C. Y.; Nanayakkara, A.; Challacombe, M.; Gill, P. M. W.; Johnson, B.; Chen, W.; Wong, M. W.; Gonzalez, C.; Pople, J. A. *Gaussian 03 (vers. B.05)*; Gaussian, Inc.: Pittsburgh, PA, 2003.

(13) Becke, A. D. *J. Chem. Phys.* **1993**, *98*, 5648−5652.

(14) Stephens, P. J.; Devlin, F. J.; Chabalowski, C. F.; Frisch, M. J. *J. Phys. Chem.* **1994**, *98*, 11623−11627.

(15) Andrae, D.; Häussermann, U.; Dolg, M.; Stoll, H.; Preuss, H. *Theor. Chim. Acta* **1990**, *77*, 123−141.

(16) Bergner, A.; Dolg, M.; Küchle, W.; Stoll, H.; Preuss, H. *Mol. Phys.* **1993**, *80*, 1431−1441.

(17) von Niessen, W.; Schirmer, J.; Cederbaum, L. S. *Comput. Phys. Rep.* **1984**, *1*, 57−125.

(18) Zakrzewski, V. G.; Ortiz, J. V.; Nichols, J. A.; Heryadi, D.; Yeager, D. L.; Golab, J. T. *Int. J. Quantum Chem*. **1996**, *60*, 29−36.

(19) Pis Diez, R. *MullPop*; National University of La Plata: La Plata, 2003.

(20) Schmidt, M. W.; Baldridge, K. K.; Boatz, J. A.; Elbert, S. T.; Gordon, M. S.; Jensen, J. H.; Koseki, S.; Matsunaga, N.; Nguyen, K. A.; Su, S. J.; Windus, T. L.; Dupuis, M.; Montgomery, J. A. *J. Comput. Chem*. **1993**, *14*, 1347−1363.

(21) Lindsay, B. G.; McDonald, K. F.; Yu, W. S.; Stebbings, R. F. *J. Chem. Phys.* **2004**, *121*, 1350−1356.

(22) Martínez, R.; Sierra, B.; Redondo, C.; Sánchez Rayo, M. N.; Castaño, F. *J. Chem. Phys.* **2004**, *121*, 11653−11660.

(23) Basner, R.; Schmidt, M.; Becker, K.; Tarnovsky, V.; Deutsch, H. *Thin Solid Films* **2000**, *374*, 291−297.

(24) Monnom, G.; Gaucherel, P.; Paparoditis, C. *J. Phys. (Paris)* **1984**, *45*, 77−84.

(25) Shul, R. J.; Freund, R. S.; Wetzel, R. C. *Phys. Rev. A* **1990**, *41*, 5856−5860.

(26) Rao, M. V. V. S.; Srivastava, S. K. *J. Geophys. Res.* **1991**, *96*, 17563−17567.

(27) Lindsay, B. G.; Rejoub, R.; Stebbings, R. F. *J. Chem. Phys.* **2003**, *118*, 5894−5900.

(28) Hudson, J. E.; Vallance, C.; Harland, P. W. *J. Phys. B: At., Mol. Opt. Phys.* **2004**, *37*, 445−455.

(29) Belić, D. S.; Kurepa, M. V. *Fizika* **1985**, *17*, 117−127.

(30) Rao, M. V. V. S.; Srivastava, S. K. *J. Geophys. Res., [Planets]* **1993**, *98*, 13137−13145.

(31) Rejoub, R.; Lindsay, B. G.; Stebbings, R. F. *J. Chem. Phys.* **2002**, *117*, 6450−6454.

(32) Jiao, C. Q.; DeJoseph, C. A., Jr.; Haaland, P.; Garscadden, A. *Int. J. Mass Spectrom.* **2000**, *202*, 345−349.

(33) Basner, R.; Foest, R.; Schmidt, M.; Becker, K.; Deutsch, H. *Int. J. Mass Spectrom.* **1998**, *176*, 245−252.

(34) Jiao, C. Q.; DeJoseph, C. A., Jr.; Garscadden, A. *Int. J. Mass Spectrom.* **2004**, *235*, 83−89.

(35) Beran, J. A.; Kevan, L. *J. Phys. Chem.* **1969**, *73*, 3866−3876.

(36) Grabandt, O.; Mooyman, R.; de Lange, C. A. *Chem. Phys.* **1990**, *143*, 227−238.

(37) Martin, W. C.; Musgrove, A.; Kotochigova, S.; Sansonetti, J. E. *Ground Levels and Ionization Energies for the Neutral Atoms*; Sept. 2003; National Institute of Standards and Technology: http://physics.nist.gov/PhysRefData/IonEnergy/ionEnergy.html.

(38) Atkins, P. W. *Physical Chemistry*; W. H. Freeman and Co.: San Francisco, 1978.

(39) Gordon, E. F.; Muddiman, D. C. *J. Mass Spectrom.* **2001**, *36*, 195−203.

(40) Cody, R. B.; Kinsinger, J. A.; Goodman, S. D. *Anal. Chem.* **1987**, *59*, 2567−2569.

(41) Verdun, F. R.; Ricca, T. L.; Marshall, A. G. *Appl. Spectrosc.* **1988**, *42*, 199−203.

(42) Schweikhard, L.; Alber, G. M.; Marshall, A. G. *J. Am. Soc. Mass Spectrom.* **1993**, *4*, 177−181.

(43) *CRC Handbook of Chemistry and Physics*, 84th ed.; Lide, D. R., Ed.; CRC Press: Boca Raton, FL, 2004.

(44) Su, T.; Bowers, M. T. In *Gas-Phase Ion Chemistry*; Bowers, M. T., Ed.; Academic: New York, 1979; Vol. 1; pp 83−118.

(45) Scott, G. E.; Irikura, K. K. *Surf. Interface Anal.* **2005**, in press.

(46) Stevens, W. J.; Krauss, M.; Basch, H.; Jasien, P. G. *Can. J. Chem.* **1992**, *70*, 612−630.

(47) Wadt, W. R.; Hay, P. J. *J. Chem. Phys.* **1985**, *82*, 284−298.

(48) Kimura, K.; Katsumata, S.; Achiba, Y.; Yamazaki, T.; Iwata, S. *Handbook of HeI Photoelectron Spectra of Fundamental Organic Molecules*; Japan Scientific Societies: Tokyo, 1981.

(49) Griffiths, W. J.; Harris, F. M.; Andrews, S. R.; Parry, D. E. *Int. J. Mass Spectrom. Ion Proc.* **1992**, *112*, 45−61.

(50) Grant, R. P.; Harris, F. M.; Andrews, S. R.; Parry, D. E. *Int. J. Mass Spectrom. Ion Proc.* **1995**, *142*, 117−124.

(51) Bancroft, G. M.; Pellach, E.; Tse, J. S. *Inorg. Chem.* **1982**, *21*, 2950−2955.

(52) von Niessen, W.; Åsbrink, L.; Bieri, G. *J. Electron Spectrosc. Relat. Phenom.* **1982**, *26*, 173−201.

(53) Grant, R. P.; Andrews, S. R.; Parry, D. E.; Harris, F. M. *Rapid Commun. Mass Spectrom.* **1998**, *12*, 382−388.

(54) Bulgin, D. K.; Dyke, J. M.; Morris, A. *J. Chem. Soc., Faraday Trans. 2* **1976**, *72*, 2225−2232.

(55) Wang, L.-S.; Niu, B.; Lee, Y. T.; Shirley, D. A.; Ghelichkhani, E.; Grant, E. R. *J. Chem. Phys.* **1990**, *93*, 6327−6333.

(56) Dyke, J. M.; Elbel, S.; Morris, A.; Stevens, J. C. H. *J. Chem. Soc., Faraday Trans. 2* **1986**, *82*, 637−645.

(57) Mazumdar, S.; Marathe, V. R.; Kumar, S. V. K.; Mathur, D. *Int. J. Mass Spectrom. Ion Proc.* **1988**, *86*, 351−355.

(58) Cesar, A.; Ågren, H.; Naves de Brito, A.; Svensson, S.; Karlsson, L.; Keane, M. P.; Wannberg, B.; Baltzer, P.; Fournier, P. G.; Fournier, J. *J. Chem. Phys.* **1990**, *93*, 918−931.

(59) Vass, G.; Tarczay, G.; Magyarfalvi, G.; Bödi, A.; Szepes, L. *Organometallics* **2002**, *21*, 2751−2757.

(60) Barker, G. K.; Lappert, M. F.; Pedley, J. B.; Sharp, G. J.; Westwood, N. P. C. *J. Chem. Soc. Dalton Trans*. **1975**, 1765−1771.

(61) Ibuki, T.; Hiraya, A.; Shobatake, K.; Matsumi, Y.; Kawasaki, M. *Chem. Phys. Lett.* **1989**, *160*, 152−156.

(62) Starzewski, K. A. O.; Dieck, H. T.; Bock, H. *J. Organomet. Chem.* **1974**, *65*, 311−325.

(63) Creber, D. K.; Bancroft, G. M. *Inorg. Chem.* **1980**, *19*, 643−648.

CT050077J